Heliyon 8 (2022) e10331

Contents lists available at ScienceDirect

Heliyon

journal homepage: www.cell.com/heliyon

Research article

Synthesis and characterization of copper zinc iron sulphide (CZFS) thin films

Joseph Onyeka Emegha [a,*], Kingsley Eghonghon Ukhurebor [b], Uyiosa Osagie Aigbe [c], John Damisa [d], Adeoye Victor Babalola [e]

[a] College of Natural and Applied Sciences, Novena University, Ogume, Delta State, Nigeria
[b] Department of Physics, Faculty of Science, Edo State University, Uzairue, Edo State, Nigeria
[c] Department of Mathematics and Physics, Faculty of Applied Sciences, Cape Peninsula University of Technology, Cape Town, South Africa
[d] Department of Physics, Faculty of Physical Sciences, University of Benin, Edo State, Nigeria
[e] Nile University of Nigeria, Research and Institution Area, Jabi-Abuja, FCT, Nigeria

ARTICLE INFO

Keywords:
Substrates
Optical
Thin films
Bandgap
Transmittance
Chemical bath deposition
Deposition time

ABSTRACT

In an aqueous bath, quaternary thin films (TFs) of copper zinc iron sulphide (CZFS) were deposited on glass (soda-lime) substrates. The present study aimed to analyse the effect of deposition periods on the properties of the prepared CZFS TFs using Chemical bath deposition (CBD). The precursor and films were examined by Fourier Transform Infrared (FTIR) spectroscopy to check for the chemical formation present. Rutherford backscattering spectroscopy (RBS) was used to determine the elemental compositions and stoichiometry of the deposited films. The optical characteristics were observed by a UV-Vis Spectrophotometer and a four-point probe (FPP) for the electrical properties. The optical characterization revealed a direct transition band-gap energy that decreased from 1.96 to 1.50 eV with an increase in deposition period. The optical constants were studied with respect to the wavelength within the range of 300–900 nm. The films exhibited high resistive properties with a conductivity that varied with an increase in deposition period. The effect of deposition periods on the optical properties of refractive index, extinction coefficient, and real and imaginary parts of dielectric constants has been reported. All these parameters were found to increase with deposition period except for the film deposited for 18 h (C3). These results confirm that the aqueous deposited CZFS films can be tuned for various optoelectronic applications.

1. Introduction

The investigation of semiconducting materials has become part of the work of many research groups due to their ease in adjusting their bandgap and physical parameters for device applications. In particular, copper and zinc chalcogenide thin films are potential semiconductor materials for solar cell fabrication, light-emitting diodes (LEDs), plasma display devices, lasers and sensors [1, 2, 3]. The accessibility of copper, zinc, and sulphur in the earth's crust makes the materials readily available [4]. Nonetheless, researchers are finding it difficult to comprehend the process of depositing ternary copper-zinc sulphide thin films due to the inappropriateness of the two cations in the sulphide system [5]. Naturally, the copper sulphide and zinc sulphide minerals have poor or absent solubility, even though they are usually linked with most ore [6]. Certainly, copper content in sphalerite is limited by weight to about 1%, and it is influenced by the presence of trivalent cations such as Ga^{3+}, Al^{3+}, In^{3+} and Fe^{3+}. Besides the difficulty of dissimilarities in the crystal structure, one more difficulty is the formation of defect complexes, which could destroy the charge carriers [7]. Additionally, the problem of the creation of highly disordered phases and structures, as well as the crystalline dupability, could be significantly different, and, therefore, so are their characteristic charge compensation mechanisms [7]. Owing to these indications, the redox property of copper in the sulphide system seems to play a decisive role in limiting the stability of the structures thermodynamically, which could be overcome by adding transition elements as impurities.

Reports on the fabrication and characterization of various ternary copper-zinc-sulphide TFs using different deposition techniques are relatively common in the literature [8, 9, 10], but work on their quaternary compounds such as CuZn(Sn, In, Fe, Pb, Ga)S is less common. In this work, we investigate the effect of the deposition period on the properties of CZFS TFs using the chemical bath deposition (CBD) technique. The

* Corresponding author.
E-mail address: jjjemegha@yahoo.com (J.O. Emegha).

https://doi.org/10.1016/j.heliyon.2022.e10331
Received 19 April 2022; Received in revised form 22 May 2022; Accepted 12 August 2022

versatility of the CBD method has led to its choice as the major deposition method for the fabrication of TFs and coatings for various applications [11, 12]. The interest in quaternary materials comes from the possibility of engineering the compound parameters with deposition. Then again, quaternary compounds are attracting increasing attention due to their good performances with moderately simple chemistry and the absence of environmental concerns associated with their uses. Even though quaternary chalcogenide materials have been fabricated, there is limited study on the growth and characterization of CZFS TFs. This research presents the synthesis of the quaternary CZFS thin films via the CBD technique. In addition, the effects of the deposition period on the morphology and optical properties of the CZFS TFs were studied and examined.

2. Materials and method

2.1. Experimental procedures and characterization

CBD was used to create copper zinc iron sulphide TFs from copper (II) chloride dehydrate ($CuCl._2H_2O$) [Assay, % purity = 99.0%], zinc chloride ($ZnCl_2$) [BDH, % purity = 99.0%], iron (III) chloride ($FeCl_3$) [PubChem, % purity = 99.0%], thiourea ($CS(NH_2)_2$) [LABOSI, % purity = 98.0%], triethanolamine [TEA] ($C_6H_{15}NO_3$) [Stenfy Chemicals, % purity = 99.0%], ammonia solution (NH_4OH) [Alfa India, 25%], and ethylenediaminetetraacetic acid [ArochemPvt. % purity = 98.0%]. The chemicals are all analytic and applied without additional purification. In this experiment, 0.5 M of $CuCl.2H_2O$ (20 ml), 0.5 M of $ZnCl_2$ (20 ml), 0.1 M of $FeCl_3$ (20 ml) and 0.2 M of CS $(NH_2)_2$ (50 ml) were mixed in distilled water in the ratio of 2:1:1:2. The complexing agents (TEA and EDTA) were employed to slow down the formative reactions, along with an ammonia solution that stabilizes the pH of the bath at 10.0. The solution was stirred for 45 min at normal room temperature to produce a uniform solution using a magnetic stirrer. Then, the substrates (soda-lime glass) were dipped into the aqueous bath in a vertical position. The reaction periods of 12, 15 and 18 h were set and tagged as C1, C2 and C3. Thereafter, the substrates were washed and dried at room temperature.

The deposited CZFS films have good adherent properties to the soda-lime substrates. Fourier transform infra-red (FTIR) spectroscopy of the precursors and films was done using a Shimadzu 8400 FTIR Spectrometer. The structural morphology was examined using the Scanning electron microscopy (SEM) system of model JEOL JSM-7600 operating at 1000 V. Rutherford backscattering spectroscopy (RBS) procedure was employed in determining the elemental compositions of the films. The optical measurements of the films were done using a UV-1800 Spectrophotometer at room temperature and wavelengths of 300–900 nm. The bandgap energy (E_g), absorption coefficient (α) and refractive index (n) were determined from the optical records. The electrical measurement was done with a four-point probe (FPP) method at room temperature.

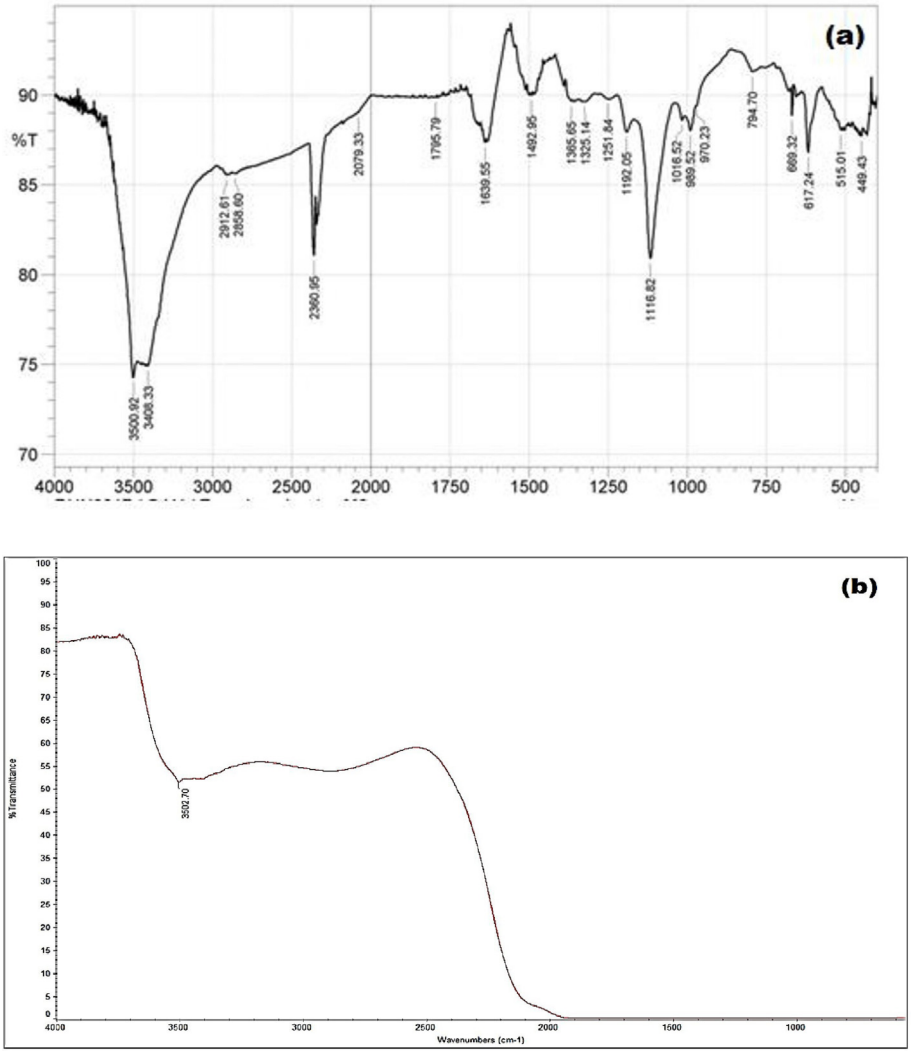

Figure 1. Infrared spectrum of CZFS (a) precursor and (b) Sample C1.

3. Results and discussion

Figure 1(a) indicates the infrared spectrum of the CZFS precursor as well as the expected absorption bands. The spectrum shows that the CZFS bonding was below the 1000 cm^{-1} mark. The O–H and N–H bands have peaks at 3500.92 cm^{-1} and 3408.33 cm^{-1}, respectively. Other major spectra include-H stretching vibrations between 2912.61 and 2360.96cm^{-1}. The regions ranging from 2000 to 1600 cm^{-1} are related to the weak sharp combinations bands, which could be the result of the polar bonds associated with the C=C vibrations [4]. The band observed

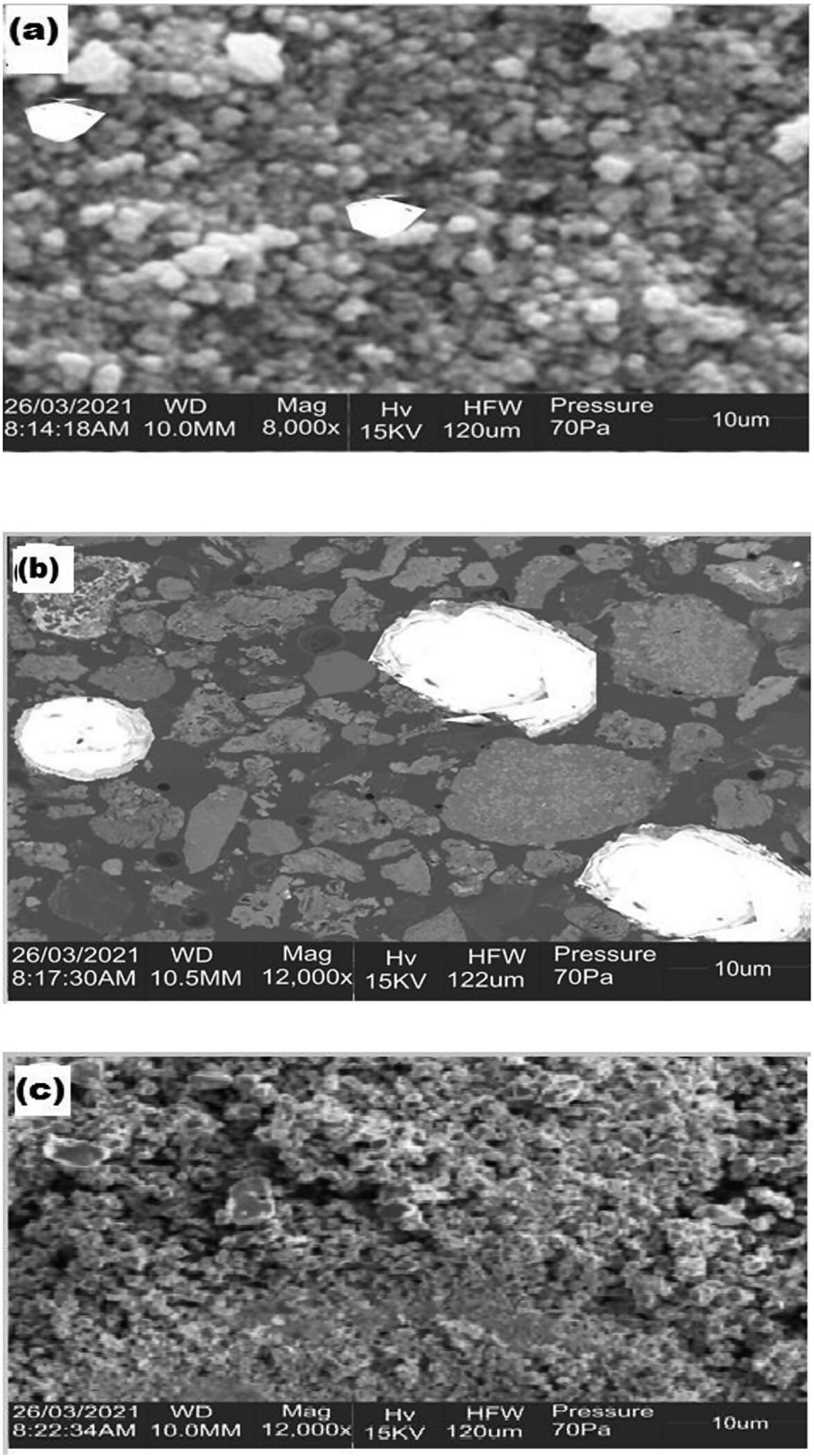

Figure 2. SEM of CZFS thin films of (a) C1, (b) C2 and (c) C3.

at 1492.96 cm^{-1} was attributed to the C=O stretching mode. Bands formed at 1400 and 1250 cm^{-1} are linked to C–H bending vibrations, as well as bands at 1116.82 and 1016.52 cm^{-1} originating from the C–C vibrations. Similar observations have been made in the literature for metal-metal semiconducting thin films [1, 4].

Figure 1(b) shows the infrared spectra of the deposited CZFS TFs at 12 h (Sample C1). The figures reveal no trace of the characteristic band associated with the precursor, which suggests a complete deposition of the precursor to yield CZFS TFs [4]. The result is comparable to metal-metal sulphide thin films reported in the literature [1, 13, 14]. Other CZFS TFs, (Samples C2 and C3) have similar characteristics. However, the visible bands at 3500 cm^{-1} may perhaps be linked to the presence of hydroxide ions within the deposited films [15].

3.1. SEM analysis

Figure 2 shows the surface morphologies of CZFS TFs at various deposition periods. From the surface morphology, it is clear that the

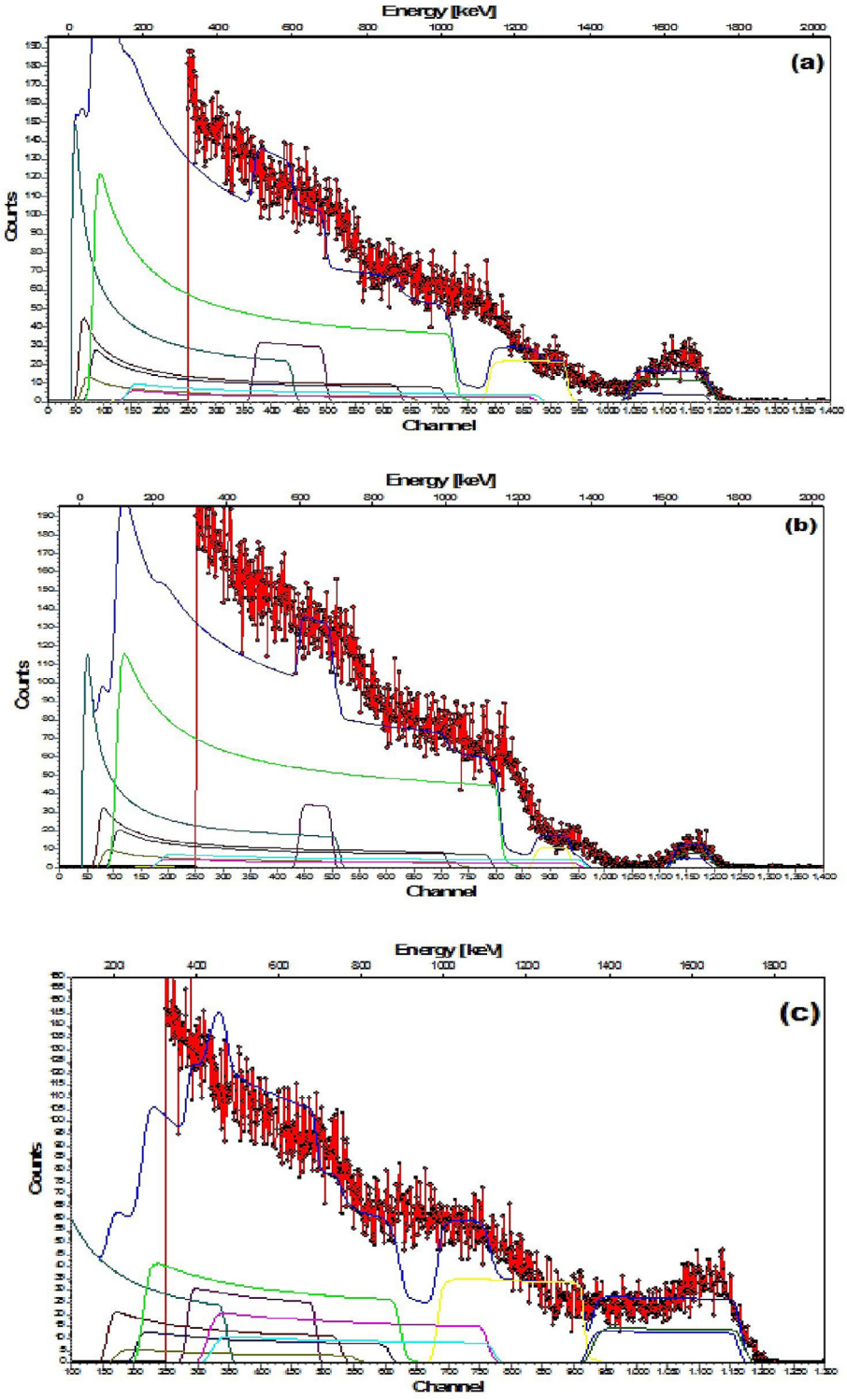

Figure 3. RBS spectrum of CZFS thin films at (a) C1, (b) C2 and (c) C3.

deposition time influences the phases exhibited by the films. Partially dense and compact nano-grains covering parts of the substrates are formed for C1 (Figure 2(a)). As the deposition time increases, the nano-grains increase in size with an agglomeration of clusters into larger grains, as indicated in Figure 2(b) for C2. After 18 h (Figure 2(c)), the clusters of larger grains metamorphose into large numbers of particle-like, rough, and irregular grains. The main explanation was that the deposition time not only reduces the defects in the material structures but also increases the crystalline (grain) roughness. This rough morphology is beneficial for photovoltaic production as rough edges attract more photons and increase the absorption and current densities within the system [16].

3.2. Elemental analysis of CZFS thin films

The chemical composition and purity of the samples are ascertained by the RBS study, which indicates the presence of copper (Cu), zinc (Zn), iron (Fe) and sulphur (S) as the elemental components within the deposited films. The normal RBS spectra of CZFS thin films are shown in Figure 3(a-c). The characteristic composition of the films is presented in Table 1, as well as the composition of the starting solutions in brackets. From the elemental analysis of the deposited films and starting solutions, it was noted that the metals-to-sulphide ratios in the starting solutions were not preserved in the films. This can be credited to the breakdown and successive reconstitution of the metal-metal-sulphide bonds during deposition due to an increase in the deposition time of the samples. Table 1 obviously reveals that the intensity of sulphur increases with the rise in deposition time, which indicates that the deposited CZFS TFs are anion rich. Therefore, the increase in deposition time has a dominant effect on the physical properties of CZFS thin films. Also, it was observed that the ratio of S/(Cu + Zn + Fe) in the CZFS-system is not constant as the deposition time is increasing, which suggests that the deposited material is non-stoichiometric. Notably, it is reasonable to assume that the elevation of deposition time induces the rate of nucleation within the atoms of the starting solution and therefore the elements in CZFS thin films, as indicated in the various morphologies in the SEM measurements [4, 13].

3.3. Optical measurements

To ascertain the suitability of the CZFS TFs for various device applications, absorbance (within 300–900 nm) was investigated at room temperature. At the reference beam, all measurements were performed on blank (clean) substrates. The absorbance spectra against wavelength are demonstrated in Figure 4. The plot confirms a strong absorption within the 300–450 nm regions. Afterwards, it falls sharply with an increase in wavelength continuously to about 900 nm. The absorption also decreases with an increase in the deposition period. This may be attributed to the perfection and improvement in crystalline sizes in the CZFS thin films [17, 18]. Comparable observations have been detailed in the literature for metal chalcogenide thin films [13, 19].

Figure 5 illustrates the variation of transmittance against the wavelength of the CZFS thin films. The plot revealed that the transmittance consists of two main regions: The first region (between 300 and 450 nm) is characterized by a comparatively lower transmittance that is increasing from about 0.6 to 0.75 as the wavelength is increasing. The

Table 1. The elemental analysis of CZFS TFs.

Samples	Elemental Composition (%)				S/(Cu + Zn + Fe)
	Cu	Zn	Fe	S	
C1	30.66 (40)	14.92 (20)	15.20 (20)	39.22 (40)	6.45
C2	29.02 (40)	12.98 (20)	14.52 (20)	43.48 (40)	7.69
C3	30.53 (40)	09.64 (20)	16.03 (20)	43.81 (40)	7.80

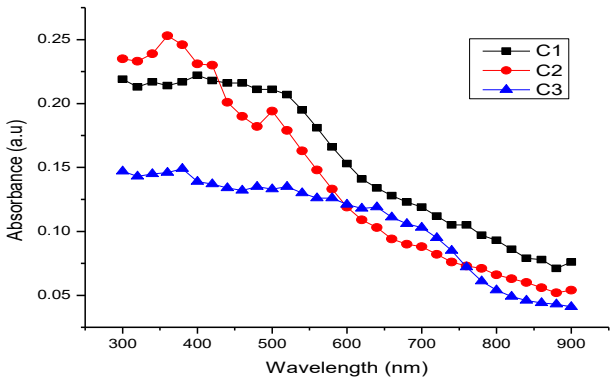

Figure 4. Absorbance spectrum of CZFS TFs.

second region (>600 nm) is characterized by higher transmittance, confirming the smooth-like nature of the deposited films. In addition, Figure 4 shows a significant increase in the transmitting properties of all the CZFS TFs, with the highest being 0.91 (91% for C3), and the lowest is found to be 0.85 (85% for sample C2). Generally, the transmittance considerably rises with an increase in the time of deposition. Low scattering and absorption losses within the CZFS system contribute significantly to the elevated transmittance observed in this study [13, 20]. It could also be a result of the increase in the period of deposition, which restructures the crystalline sizes and, thus, improves the transmittance of the deposited films, as indicated by the SEM studies. The elevated transmittance within the spectra range indicated in Figure 4 makes CZFS thin films a good conducting material for solar cells, pyro-electric detectors, and LED applications [4, 21].

According to the solid-band theory, the (direct) bandgap (E_g) for semiconductor materials is determined using the following expression [11, 18]:

$$\alpha = \left(\frac{A}{h\nu}\right)\left[h\nu - E_g\right]^n \quad (1)$$

When $n = 0.5$.

Recall that $0.5 = \frac{5}{10} = \frac{1}{2}$,

Therefore; $\alpha = \frac{A}{h\nu}(h\nu - Eg)^{\frac{1}{2}}$

$\alpha h\nu = A\ (h\nu - Eg)^{\frac{1}{2}}$

Squaring both sides, $(\alpha h\nu)^2 = A\ (h\nu - Eg)$

where A is a constant. Therefore, the plot of $(\alpha h\nu)^2$ against hν, when $(\alpha h\nu)^2 = 0$ gives the band-gap of the material [13, 14, 15, 19]. Here, α, hν, E_g are the absorption coefficient, photon energy, and bandgap respectively. Also, from Eq. (1), "A" characterizes an energy-dependent constant and the index n has a size of 0.5 [1]. Figure 6 presents the notable Tauc plots of $(\alpha h\nu)^2$ versus $(h\nu)$ for all the films based on Eq. (1) [13, 14, 15, 19]. The E_g was estimated by extrapolating the linear section of the plot onto the x-axis. The E_g varies from 1.30 to 1.78 eV with an increase in the period of deposition. Interestingly, numerous factors are responsible for the variation in the estimated E_g values. Among these is the fact that the nature of CZFS thin films results in films with larger crystalline sizes with a rise in deposition time. Accordingly, the E_g of the material tends to fall as the deposition period is increased, owing to growth in the crystalline sizes [18]. It is also suggested that the band trailing initiated by the disorder within the CZFS system of the films contributes significantly to the variations in the E_g values [21]. Furthermore, the effects of impurities and defects, transition tail, shift effects, and residual strain all have a significant impact on the Eg of a semiconductor thin film system [13, 21]. Still, the varying E_g due to deposition durations makes the films beneficial for solar cell fabrication, as a result of

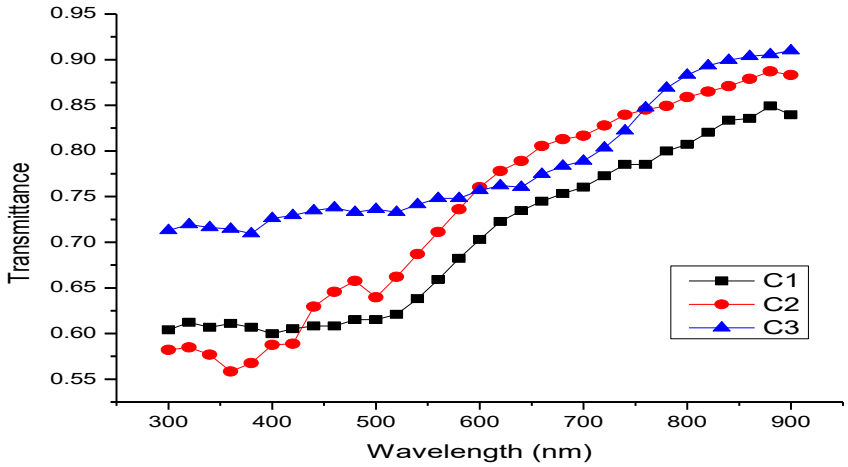

Figure 5. Transmittance spectrum of CZFS TFs.

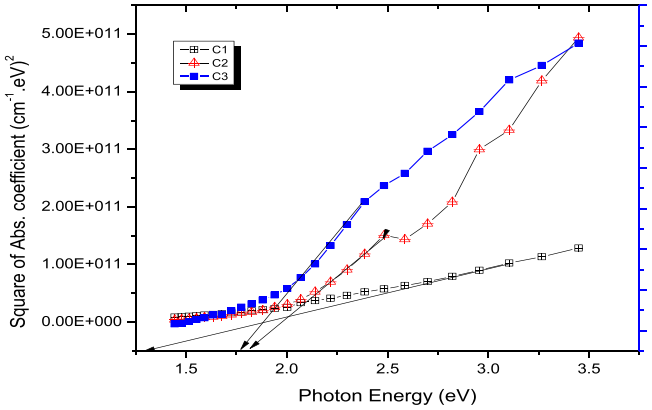

Figure 6. Band-gap values of CZFS TFs.

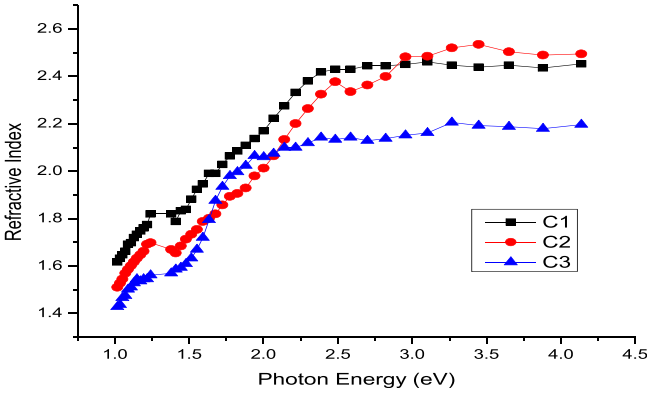

Figure 7. Refractive Index and photon energy of CZFS TFs.

allowing more photons to have access to the absorbing films and creating more photocurrents [4, 22].

Determining the refractive index (n) of a material is a central consideration in the building-up of many optical devices like modulators, switches, filters, waveguides, detectors, solar cells, etc., owing to its close connection with the electronic polarization of the material [23, 24, 25]. Usually, n is related to the polarization (electronic) of ions and is evaluated using the following relation in Eq. (2) [26]:

$$n = \left(\frac{1+R}{1-R}\right) + \sqrt{\left(\frac{4R}{(1-R)^2}\right) - k^2} \tag{2}$$

Respectively, R and k are the reflectance and the extinction coefficient. The graph of n versus the photon energy is shown in Figure 7. From the plot, it is seen that the average n increased with the CZFS TFs photon energy. C2 has the highest (average) refractive index of 2.51 at 3.5 eV. Nonetheless, as the deposition time is increased, the refractive indexes were found to alternate within the range of 2.19 and 2.51 at 3.5 eV. These changes evident in the n-values may be due to the trapped photon energy within the grain boundary system of the films [4]. The high n-values of CZFS films could be used to improve the visual properties of various optoelectronic applications such as quantum dot light-emitting diodes (QDLED) and liquid crystal displays (LCD), where electronic display mechanisms are needed [26].

For semiconductors, the extinction coefficient (k) is calculated using the expression in Eq. (3) [14]:

$$k = \frac{\alpha\lambda}{4\pi} \tag{3}$$

Here, α and λ expresses the absorption coefficient and wavelength of the spectrum. The plot of k against photon energy is indicated in Figure 8. It is observed that k increases with photon energy as well as with deposition time for all the films as indicated in the Figure (Figure 8). Generally, the estimated values of the extinction coefficients were low over the photon energy (eV) regions, consequently losing very low absorption energy down the regions [4].

The optical dielectric constants (real and imaginary parts) are directly related to the electronic structure and the density of states within the energy gap of the CZFS films [14]. These constants are determined by the following relations, indicated in Eqs. (4) and (5) [13, 23].

$$\varepsilon_r = n^2 - k^2 \tag{4}$$

and

$$\varepsilon_r = 2nk \tag{5}$$

where ε_r and ε_i are the real and imaginary dielectric constants. The plot of the ε_r and ε_i against photon energy is shown in Figures 9 and 10 respectively. Figure 9 reveals that the real dielectric constants are increasing with photon energy as well as with the deposition time.

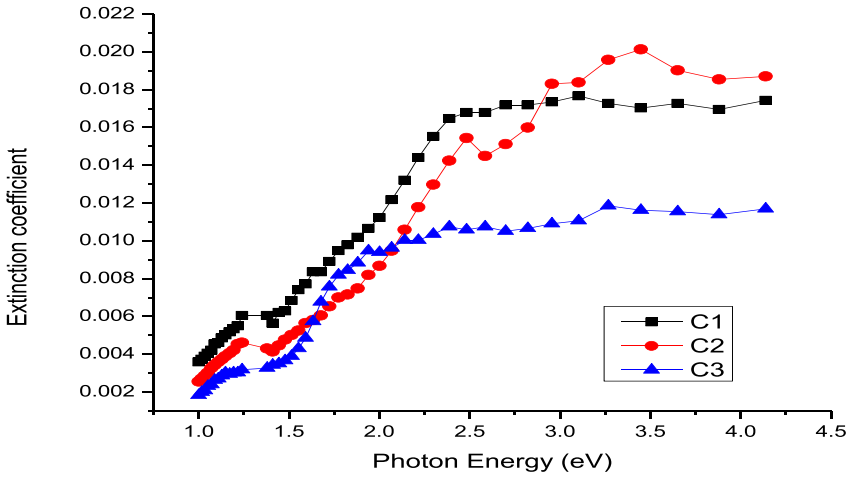

Figure 8. Extinction Coefficient and photon energy of CZFS TFs.

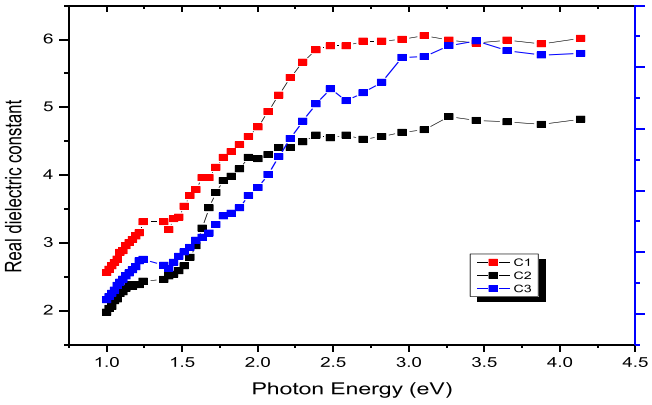

Figure 9. Real dielectric constant and photon energy of CZFS TFs.

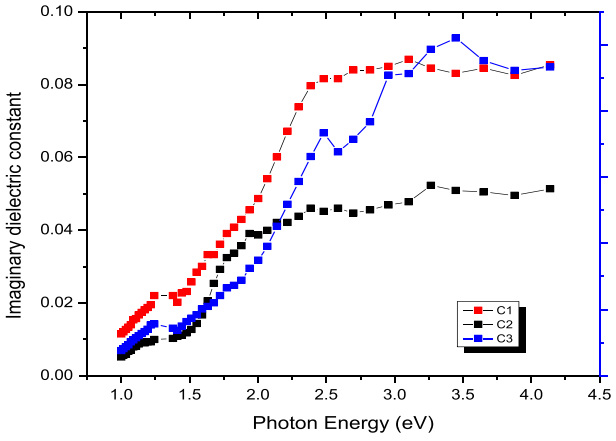

Figure 10. Imaginary dielectric constant and photon energy of CZFS TFs.

However, C2 has the lowest value of 4.5 at photon energy of 3.5 eV. The behaviour may be associated with the nature of the film (C2), which has the least speed when agitated with electromagnetic radiation [27]. A similar trend has been outlined by Efe et al. [13] and Olofinjana et al. [14] for crystalline semiconductor thin films and linked the development to the connections between the real constant (ε_r), refractive index (n) and the extinction coefficient (k) as indicated by Eq. (4).

The increment in the ε_i against photon energy is indicated in Figure 10. The figure reveals that the films increase sharply with deposition time along with the photon energy range. Generally, the films exhibited low imaginary dielectric constant values when compared to the real dielectric constant. Furthermore, sample C3 has a relatively higher value of 0.09 at the long photon energy range, while sample C2 has the least of about 0.05 (Figure 10). The variations observed in the imaginary dielectric values may be a sign of the energy-absorbing nature of the deposited CZFS thin films within a charged region [27].

3.4. Current-voltage (I–V) analysis

The resistivity results were determined using the FPP measurements. The current-voltage (I–V) readings were taken several times to reduce errors in the measurements. The average values of the I–V were recorded and used to determine the sheet resistance (R_s) according to the relation in Eq. (6) [28];

$$R_s = \frac{\pi}{\ln 2}\left(\frac{V}{I}\right) \tag{6}$$

The resistivity (ρ) of the films was evaluated by multiplying the R_s with the various thicknesses. Furthermore, the conductivity (σ) was obtained from the inverse of the resistivity. The summary of the determined electrical properties and thickness are listed in Table 2. It was observed that the deposition period has a great effect on the electrical properties of CZFS TFs, as the sheet resistances were found to be high for all the films. The high sheet resistance may result from the high impurity content within the CZFS system [28] and increased deposition time. The reason is connected to the swift production of more pairs of charge-carriers (electrons and holes) within the CZFS system occasioned by the increase in deposition time [17]. Hence, the determined values of the electrical conductivity confirm the semiconducting nature of the deposited CZFS thin films [19, 28].

Typically, the conductivity nature of semiconducting thin films is dependent on the thickness and crystalline nature of the material [28]. Consequently, in CZFS thin films, the increase in electrical conductivity were due to the increase in both thickness and deposition time (Table 2). This indicates that limited (grain) electron-scattering will take place in C3 rather than in C1, since electron-scattering is inversely related to the electrical conductivity [19, 29], thus increasing conductivity with thickness and deposition time.

Table 2. The thickness and electrical properties of CZFS thin films.

Samples	Thickness (nm)	Sheet resistance	Resistivity	Conductivity
		$(\Omega/Sq) \times 10^6$	(Ω cm)	$(\Omega.cm)^{-1}$
C1	53.70	18.60	0.99	1.01
C2	69.52	7.25	0.50	2.00
C3	86.10	2.66	0.23	4.34

4. Conclusion

CZFS thin films at room temperatures were synthesized via the CBD technique. The CBD technique generally allows for a simplified synthesis of CZFS thin films while retaining exceptional influence over the chemical, SEM, and optical properties of the material. The FTIR and RBS results of the films indicated that the spectrum contains copper (Cu), zinc (Zn), iron (Fe) and sulphur (S) in various stoichiometry at different deposition times. The SEM observations showed that the deposited CZFS thin films consist of rough and compact nano-grains that depend on the deposition time. The films exhibited excellent absorbing and transmitting properties that varied with an increase in the wavelength (300–900 nm) and deposition times. A variation in the band gap within 1.30–1.78 eV was estimated as the deposition period was increased. The n, k, and dielectric constants (ε_r and ε_i) showed that the optical measurements of the CZFS were determined by deposition periods. Thus, the I–V measurement implies that CZFS thin films are naturally semiconducting, and there is the possibility of using CBD in depositing high-quality semiconducting films for optoelectronic device applications with comparable properties.

Since, a surface-sensitive quantitative spectroscopic method based on the photoelectric effect called X-ray photoelectron spectroscopy (XPS) can identify the elements present in a material (its elemental composition) or that are present on its surface, as well as their chemical state, general electronic structure, and density of the electronic states in the material. It is therefore suggested that future studies be conducted on XPS data (which will reveal the oxidation states of elements) as well as XPS depth profiling. Also, the EDX was not considered during this study due to limitations in the device used for the study. However, this will be considered in future scope so as to show the distribution of elements in a selected area wherein RBS measurements cannot provide such a feature.

Declarations

Author contribution statement

Joseph Onyeka Emegha: Conceived and designed the experiments; Performed the experiments.

Kingsley Eghonghon Ukhurebor, Uyiosa Osagie Aigbe: Analyzed and interpreted the data; Wrote the paper.

John Damisa: Performed the experiments.

Adeoye Victor Babalola: Contributed reagents, materials, analysis tools or data.

Funding statement

This research did not receive any specific grant from funding agencies in the public, commercial, or not-for-profit sectors.

Data availability statement

Data included in article/supplementary material/referenced in article.

Declaration of interests statement

The authors declare no conflict of interest.

Additional information

No additional information is available for this paper.

References

[1] J.O. Emegha, J. Damisa, F.O. Efe, B. Olofinjana, M.A. Eleruja, S.O. Azi, Preparation and characterization of metal organic chemical vapour deposited copper zinc sulphide thin films using single solid source precursor, Eur. J. Mater. Sci. Eng. 4 (1) (2019) 11–22.

[2] S.H. Mohamed, Photocatalytic, optical and electrical properties of copper-doped zinc sulfide thin film, J. Phys. D Appl. Phys. 43 (3) (2010), 35406.

[3] R. Vishwakarma, Effect of substrate temperature on ZnS films prepared by thermal evaporation technique, J TheorAppl Phys 9 (2015) 185–192.

[4] J.O. Emegha, C.M. Okafor, K.E. Ukhurebor, Optical properties of copper-zinc sulphide network from mixed single solid source precursors of copper and zinc dithiocarbamate, Walaika J. Sci. Technol. 18 (9) (2021) 1–11.

[5] A. Short, L. Jewell, A. Bielecki, T. Keiber, F. Bridges, S. Carter, G. Alers, Structure in multilayer films of zinc sulfide and copper sulfide via atomic layer deposition, J. Vac. Sci. Technol. 32 (2014) 1–8, 01A125.

[6] M. Innocenti, L. Becucci, I. Bencista, E. Carretti, S. Cinotti, L. Dei, F. Di Benedetto, A. Lavachi, F. Marinelli, E. Salvietti, F. Vizza, M.L. Foresti, Electrochemical growth of Cu-Zn sulfides, J. Electroanal. Chem. 710 (2013) 17–21.

[7] L. Wang, G.T. Barkema, H.H. Pham, DFT + U studies of Cu doping and p-type compensation in crystalline and amorphous ZnS, Phys. Chem. Chem. Phys. 1 (2015) 1–16.

[8] C.C. Uhuegbu, E.B. Babatunde, C.O. Oluwafemi, The study of copper zinc sulphide ($CuZnS_2$) thin film, Turk. J. Phys. 32 (2008) 39–47.

[9] E. Jose, M.C. Santhosh Kumar, Room temperature deposition of highly crystalline Cu-Zn-S thin films for solar cell applications using SILAR method, J. Alloys Compd. (2007).

[10] G. Louis, K.P. Vijayakumar, C. SudhaKartha, J. Jubimol, Analysis of spray pyrolysed Copper zinc sulfide thin film suing photoluminescence, J. Lumin. (2018).

[11] J.O. Emegha, J. Damisa, D.E. Elete, T.E. Arijaje, A. Akinpelu, P.O. Ogundile, C.A. Onumejor, Growth and characterization of copper cadmium sulphide thin film, J. Phys.: Conf. Ser. 1734 (2021), 12045.

[12] R.S. Mane, C.D. Lokhande, Chemical deposition method for metal chalcogenide thin films, Mater. Chem. Phys. 65 (2000) 1–31.

[13] F.O. Efe, B. Olofinjana, O. Fasakin, M.A. Eleruja, E.O.B. Ajayi, Composition, structural, morphological, optical and electrical property evolution in mocvd Cu-Zn-S thin films prepared at different temperature using a single solid source precursor, J. Electron. Mater. 48 (12) (2019) 1–14.

[14] B. Olofinjana, A.C. Adebisi, F.O. Efe, O. Fasakin, K.O. Oyedotun, M.A. Eleruja, E.O.B. Ajayi, N. Manyala, Single solid source precursor route to the synthesis of MOCVD Cu-Cd-S thin film, Mater. Res. Express 6 (2019).

[15] J. Damisa, B. Olofinjana, O. Ebomwonyi, F. Bakare, S.O. Azi, Morphological and optical study of thin films of $CuAlS_2$ deposited by metal organic chemical vapour deposition technique, Mater. Res. Express (4) (2017), 086412.

[16] M. Arslan, A. Habib, M. Zakri, A. Mehmood, G. Husnain, Elemental, structural and optical properties of nanocrystalline $Zn1\text{-}_xCu_xSe$ films deposited by close spaced sublimation technique, J. Sci.: Adv. Mater. Devices 2 (2017) 79–85.

[17] W.A. Al-Taa'y, S.F. Oboudi, E. Yousif, M.A. Nabi, R.M. Yusop, D. Derawi, Fabrication and characterization of nickel chloride doped PMMA film, Adv. Mater. Sci. Eng. 913260 (2015) 1–5.

[18] S. Mohato, A.K. Kar, The effect of annealing on structural, optical and photosensitive properties of electrodeposited cadmium selenide thin films, J. Sci.: Adv. Mater. Dev. 2 (2017) 165–171.

[19] J.O. Emegha, K.E. Ukhurebor, U. Aigbe, B. Olofinjana, S.O. Azi, M.A. Eleruja, Effect of deposition temperature on the properties of copper-zinc sulphide thin films using mixed copper and zinc dithiocarbamate precursors, GU J. Sci. 35 (4) (2023) 1556–1570, 2022.

[20] S. Anandan, S. Muthukumaran, Microstructural, crystallographic and optical characterizations of Cu-doped ZnO nanoparticles co-doped with Ni, J. Mater. Sci. Mater. Electron. 26 (2015) 4298–4307.

[21] J. Damisa, J.O. Emegha, I.L. Ikhioya, Deposition time induced structural and optical properties of lead tin sulphide thin films, J. Nig. Soc. Phys. Sci. 3 (2021) 455–458.

[22] R.P. Ghediya, T.K. Chaudhuri, J. Ray, H.L. Panjwani, P.J. Hemani, P.P. Paneri, R.P. Jadev, K.D. Rupapara, R.R. Joshi, Synthesis and characterization of copper cadmium sulphide (CuCdS2) as potential absorber for thin film photovoltaic, Mater. Chem. Phys. 252 (2020), 123382.

[23] A.S. Hassanien, A.A. Akl, Influence of composition on optical and dispersion parameters of thermally evaporated non-crystalline $Cd_{50}S_{50}$-xSex thin films, J. Alloys Compd. 648 (2015) 280–290.

[24] K.S. Ajay, An empirical relation showing the variation of refractive index with energy gap for $A^{1}B^{111}C2^{v1}$& $A^{11}B^{1v}C2^{v}$ type ternary semiconductor, IJIRT 5 (4) (2018) 85–88.
[25] J. Damisa, J.O. Emegha, XRD and UV-Vis Spectroscopic studies of lead tin sulphide (PbSnS) thin films, Trends Sci. 18 (20) (2021) 16.
[26] Q.M. Al-Bataineh, M. Telfah, A.A. Ahmad, A.M. Alsaad, I.A. Qattan, H. Baaziz, Z. Charifi, A. Telfah, Synthesis, crystallography, microstructure, crystal defects, optical and optoelectronics properties of ZnO: CeO_2 mixed oxide thin films, Photonics 7 (2020) 112.
[27] R.Z. Moghadam, M.H. Ehsani, H.R. Dizaji, M.R. Sazideh, Thickness dependence of structural and optical properties of CdTe films, Iran, J. Mater. Sci. Eng. 15 (2018) 3.
[28] J.O. Emegha, B. Olofinjana, K.E. Ukhurebor, J.T. Adegbite, M.A. Eleruja, Electrical properties of semiconducting copper zinc sulphide thin films, Curr. Appl. Sci. Technol. 22 (1) (2022) 1–9.
[29] F. Gode, E. Guneri, F.M. Emen, V. Emir Kafadar, S. Unlu, Synthesis, structural, optical, electrical and thermoluminescence properties of chemically deposited PbS thin films, J. Lumin. 147 (2014) 41–48.